

### N IX.3. NOISE IN INVERTER-FED SQUIRREL-CAGE INDUCTION MOTORS

RONNIE J. M. BELMANS  
*Department of ESAT/ELEN  
Katholieke Universiteit Leuven-Belgium*

CT

iction and analysis of the audible noise of inverter supplied squirrel cage motors is an electromagnetic problem. The calculation requires the input current and voltage spectrum of the inverter used to supply the variable to the motor. However, the electromagnetic design of the motor as such has n into account. Given the electrical input and the motor electromagnetic data, ; exciting the mechanical structure can be determined. In order to find out or not a high audible noise level has to be expected, the mechanical response, oretical or experimental has to be obtained. This section discusses the various he analysis and their mutual interactions. In addition several examples are strating the approach.

RDS  
oise / inverter supplied induction motor / magnetic forces / vibration

action

of inverters for controlling the speed of induction motors creates various caused by the distortion of the supplied voltage. One such problem is the dible noise level when compared with sinusoidal voltage drives. In addition, economical pressures force machine manufacturers to use less active Since the frame is less stiff, the machines become more sensitive to vibrations addition, less iron is used in the stator, again yielding a weaker structure. Less yields higher flux density distribution values. At higher field levels, the forces he audible noise increase proportionally to the squared field values [5]. applied machines have recently been installed in environments requiring quiet . i.e., in air-conditioning systems, fans and printers in personal computer etc. Therefore, a much lower audible noise level is required. he constraints encourage the designer of drives toward the use of more techniques for predicting audible noise of induction motors fed by inverters. audible noise is a combined electromechanical problem as first recognized by

an [5]. Electromagnetic forces cause the mechanical structure of the stator to vibrate. Obviously, other sources also exist in electrical machines, but they are not considered here. An example of an overall analysis including mechanical causes may be found in [6]. Most authors merely present either the mechanical [7, 8] or the magnetic aspects [9-11] of the problem. In recent years, the first papers dealing with the influence of the inverters were published [12, 13]. Several techniques described in literature, yield a prediction of the frequency components of the audible noise. They do not give information on the amplitudes of the components. The amplitudes depend on the acoustic emission quality of the inverter. This, in turn, is very difficult to predict accurately. If the audible noise is considered, it can be stated that a high level may be expected when a component of the frequency spectrum of the magnetic forces in the air gap coincides with one of the natural frequencies of the stator assembly.

**romagnetic Considerations**

**ANALYSIS OF THE INVERTER VOLTAGE**

*oretical Approach*

Analysis of the frequency spectrum of an inverter may be performed in two different ways. The first approach is offered by the analytical Fourier analysis of the voltage or current supplied by the inverter. If for instance the phase voltage of a six-step inverter is considered, the idealized time pattern of the phase voltage is known (Fig. 1).  $V_{dc}$  is the instantaneous voltage in the dc link and  $T$  is the period of the fundamental component of the inverter voltage. The Fourier series of this time pattern is

$$v(t) = \frac{2V_{dc}}{\pi} \sum_{m=1,3,5,\dots} \left[ \cos m\omega t + \frac{1}{(6m+1)} \cos 6m\omega t \right] \quad (1)$$

where  $v(t)$  is the pulsation of the fundamental component of the supplied voltage.

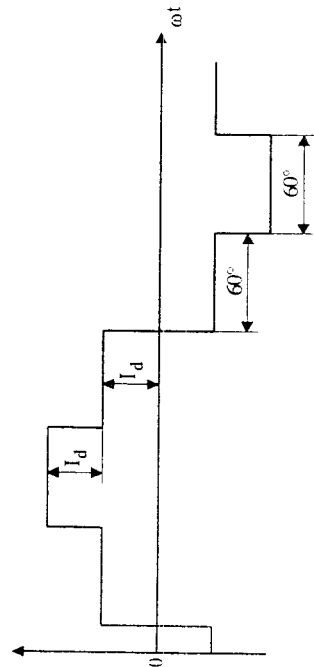


Figure 1. Phase voltage of the six-step voltage source inverter (VSI)

TABLE 1. Frequency spectrum of the six-step VSI

Number	Frequency [Hz]	Theory [%]	Experiment [%]
1	42.5	100	100
5	212.5	20	23
7	297.5	14	12
11	467.5	9	11
13	552.5	8	4
17	722.5	6	2
19	807.5	5	2

In a current source inverter (CSI) the current amplitudes are also inversely proportional to the harmonic number:

$$i_k(t) = \frac{2I_{dc}}{\pi} \sum_{m=1,3,5,\dots} \left[ \cos m\omega t + \frac{1}{(6m+1)} \cos 6m\omega t \right] \quad (2)$$

The voltage of an harmonic of the current source inverter is linked to the current by the voltage equation of the motor [12, 13]:

$$U_{(6m\pm 1)} \approx [R_1 + R_2 + j(6m \pm 1)X_{\sigma}] I_{(6m\pm 1)} \quad (3)$$

For the voltage source inverter (VSI), the inverse formulation may be used. When analyzing the frequency spectrum of various pulse-width-modulated (PWM) inverters (e.g. [14]), it becomes obvious that it is practically impossible to cover all existing modulation techniques in an analytical way. A better method of tackling this problem is the use of digital fast-Fourier transform routines, calculating the spectrum starting from the theoretical time pattern of the PWM voltage. The various approaches to modulation are treated in an other portion of this book and therefore, are not discussed here.

However, a large audible noise level is to be expected when resonance occurs, i.e. as one of the exciting frequencies coincides with one of the natural frequencies of the stator assembly. Building up the energy required to generate the high audible noise level during resonance, implies a sufficient long time. Therefore, the use of so-called random PWM, which continuously changes the frequency spectrum will avoid the audible noise problems caused by the time harmonics to a major extent.

*2.1.2. Experimental approach*

If an existing inverter is to be analyzed, an experimental approach may be used. The voltage supplied by the inverter is measured and a Fast-Fourier Transform algorithm is applied. Even with simple six-step inverters the result differs from the theoretical one, due to the non-ideal voltage (Table 1). When comparing the frequency spectra of two PWM inverters using different modulation techniques, the first one having transistor switches operating at 1.2 kHz and the second one having IGBT's at 12 kHz switching frequency, it becomes clear that the harmonic components are shifted towards the higher frequency region. These inverters are used in the experimental verification of the 13.5 kW motors.

The voltage and frequency are controlled in such a way that their ratio is kept constant ( $U/f = \text{constant}$ ). This ensures that the overall flux and therefore, the saturation level in the machine is kept the same.

Eq.3 is illustrated in the following measured curves. Fig.3 shows the current spectrum of the standard induction motor supplied by the CSI at 40 Hz, while Fig.4 gives the corresponding voltage spectrum. Figs.5 and 6 give these quantities for the same motor supplied by the VSI-PWM inverter.

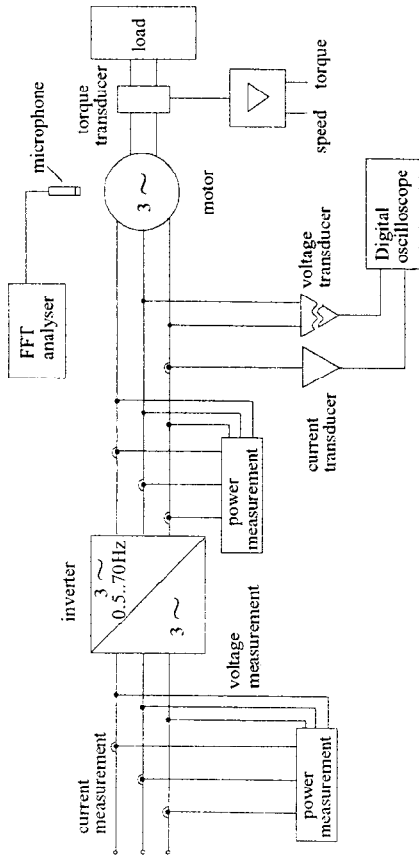


Figure 2. Lay-out of the experimental set-up

Three groups of drives are used: two 1.1 kW induction motors, different 13.5 kW motors and a series of 90 kW motors. The input currents and voltages are measured, as well as the overall audible noise. The currents, voltages and the audible noise are analyzed using a frequency analyzer (Fig.2). The audible noise is measured in a semi-echoic chamber, avoiding interference of the frequency inverter audible noise and due reflections of the walls and other material near to the set-up. The audible noise is measured using a condenser microphone. Both the overall audible noise levels in dB(A), and its frequency spectrum is registered. In the experiments of the 13.5 kW motors, a load is applied. The load has a very low audible noise level due to special bearings and water cooling.

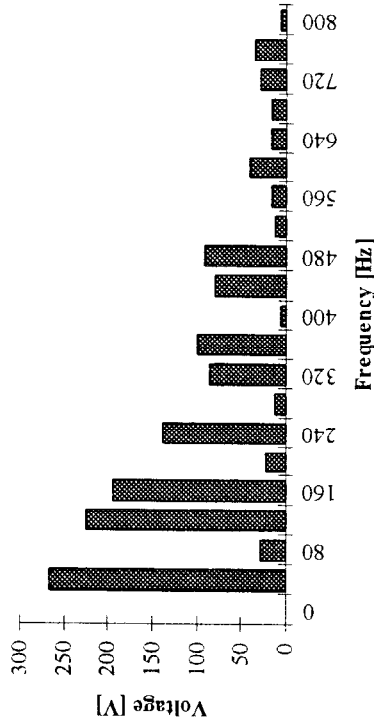


Figure 4. Voltage spectrum CSI standard squirrel cage induction motor-40 Hz

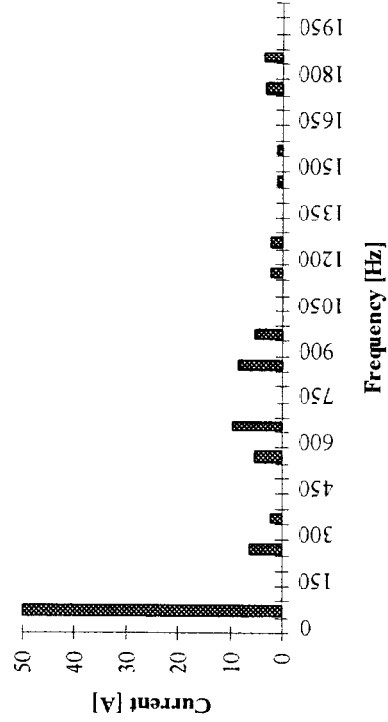


Figure 5. Current spectrum PWM-VSI-standard squirrel cage induction motor-40 Hz

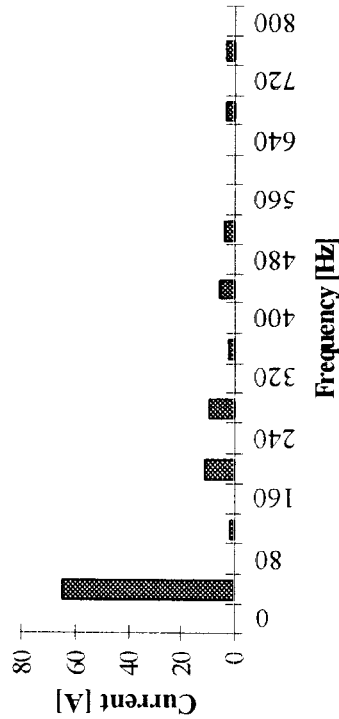


Figure 3. Current spectrum CSI standard squirrel cage induction motor-40 Hz

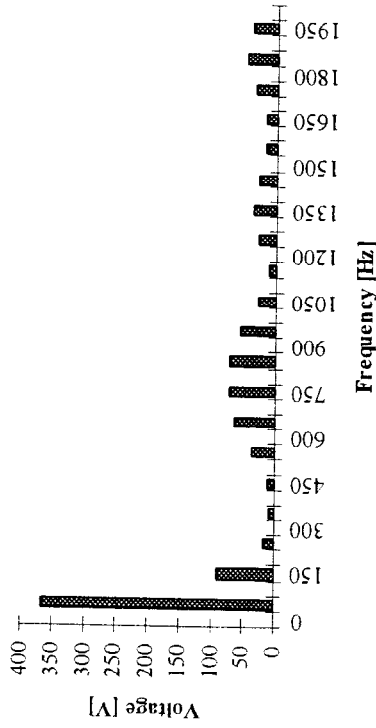


Figure 6. Voltage spectrum PWM-VSI-standard squirrel cage induction motor-40 Hz

## 4. MAGNETIC FORCES

Two different approaches for calculating the flux density distribution in the machine air gap are common:

- the distribution is regarded as the superposition of an infinite number of flux density distribution waves;
- the distribution is calculated by conformal transformation, a finite difference or finite element method, considering the slotted nature of stator and rotor.

In the induction motor, the first method is the most popular. If the influence of saturation, eccentricity and slotting is neglected, the stator flux density distribution of a symmetrical three phase winding is [5]:

$$B_{Sv}(x, t) = \sum_v B_{Sv} \cos[v\alpha - \omega_k t - \varphi_{v,k}] \quad (5)$$

where

- $B_{Sv}$  amplitude of various flux density distribution components;
- $\alpha$  angular coordinate measured from stator reference;
- $k$  number of a time harmonic;
- $v$  number of a space harmonic.

$$v = (2g+1)p \quad g = 0, \pm 1, \pm 2, \dots; \quad (6)$$

$p$  number of pole pairs of machine;

$\omega_k$  pulsation of a harmonic component of inverter voltage.

Of specific importance are the, so-called, slot harmonics that are not suppressed by the winding lay-out. These numbers are ( $Z_1$ : number of stator slots):

$$v_{slot} = p \pm gZ_1 \quad (7)$$

The rotor flux density distribution of a squirrel-cage rotor, due to the currents induced by the  $v$ -th stator space harmonic, is

$$b_{\lambda_{v,R}} = B_{\lambda_{v,R}} \cos(\lambda_{v,R}\alpha - \omega_{\lambda_{v,R}}t - \varphi_{\lambda_{v,R}}t) \quad (8)$$

with

$$\lambda_{v,R} = gZ_2 + v \quad g = 0, \pm 1, \pm 2, \dots \quad (9)$$

and

$$\omega_{\lambda_{v,R}} = \omega_k \left[ 1 + \frac{gZ_2}{p}(1 - s_k) \right] \quad (10)$$

where

$Z_2$  number of rotor bars;

$s_k$  slip of  $k$ -th time harmonic.

$$s_k = \frac{(\omega_k - \omega_m)}{\omega_k} \quad (11)$$

where  $\omega_m$  is the mechanical angular speed of machine.

The slip is practically zero when the motor is at no-load for the fundamental component of the stator voltage and is practically unity for all other time harmonics:

$$s_k = \begin{cases} 0 & \text{fundamental component} \\ 1 & \text{time harmonic} \end{cases} \quad (12)$$

Due to slotting, a sinusoidally distributed current distribution would lead to a non-sinusoidally distributed flux density distribution. The slots are exhibiting a large reluctance, while the teeth offer virtually no magnetic resistance. This provides the, so-called, slotting harmonics having the same number of pole-pairs as the slot harmonics (Eq. 7). However, their amplitude is proportional to the no-load current, and the slot harmonics have an amplitude proportional to the load current. The addition of both slot and slotting harmonics has to account for the phase angles [17]. In the measurements of the 1.1 kW and 90 kW motors discussed further on, the motors are at no-load. Therefore, slotting harmonics are more pronounced. The same holds for the rotor. This is the way the number of rotor slots enters the analysis.

Due to saturation, the effective air-gap length is not constant. If only the fundamental time harmonic component is considered, the corresponding flux density distribution wave has the triple number of pole pairs, the triple pulsation and the triple phase angle:

$$b_{\text{saturation}} = B_{\text{saturation}} \cos[3(p\alpha - \omega t - \varphi)] \quad (13)$$

If the current distribution due to a time harmonic is considered, a different type of flux density wave is generated. Saturation is defined by the fundamental and therefore, the saturation harmonic due to a higher time harmonic is [18, 19]:

$$\begin{aligned} b_{\text{saturation},k} &\approx A \sin(v\alpha - \omega_k t - \varphi_{v,k}) \Lambda \cos[2(p\alpha - \omega t - \varphi_m)] \\ &= B_{\text{sat},-} \cos[(v-2p)\alpha - (\omega_k t - 2\omega)t - (\varphi_{v,k} - 2\varphi_m)] \\ &\quad + B_{\text{sat},+} \cos[(v+2p)\alpha - (\omega_k t + 2\omega)t - (\varphi_{v,k} + 2\varphi_m)] \end{aligned} \quad (14)$$

Eccentricity can produce further harmonics as discussed in [20]. However, this type of harmonic is seldom reported to give extra audible noise.

The radial force waves  $\sigma_r$  are proportional at every point to the square of the flux density wave (Maxwell stress):

$$\sigma_r = \frac{b^2(\alpha, t)}{2\mu_0} \quad (15)$$

therefore, the combination of two magnetic flux density waves

$$b_{1,2}(x, t) = B_{1,2} \cos(p_{1,2}\alpha - \omega_{1,2}t - \varphi_{1,2}) \quad (16)$$

elds

$$\sigma_r = \frac{b_1^2(\alpha, t)}{2\mu_0} + \frac{b_2^2(\alpha, t)}{2\mu_0} + \frac{b_1(\alpha, t)b_2(\alpha, t)}{\mu_0} \quad (17)$$

Both square terms result in a constant stress and in a radial force wave having double the number of pole pairs and double the pulsation of the flux density wave generating it. The third term generates radial force waves having number of pole pairs

$$p_r = p_1 \pm p_2 \quad (18)$$

d pulsation

$$\omega_r = \omega_1 \pm \omega_2 \quad (19)$$

These pulsations compose the frequency spectrum of the audible noise emitted by machine.

In theory, an infinite number of force components results from this analysis. The following considerations are used to limit the number:

- The amplitudes of the radial force waves are proportional to the product of the amplitude of both flux waves, which are proportional to the voltage harmonics causing them. Therefore, the analysis is stopped when the relative amplitude of the time harmonic with respect to the fundamental component is less than a given value.
- The space harmonics of the flux density distribution waves are used up to the second slot harmonic. No rotor harmonics due to currents induced by the stator harmonics are considered.
- The stator does not tolerate any deformation if the number of pole pairs of the radial force wave is higher than four. Therefore, these waves are not considered.

### 2.3. PRACTICAL EXAMPLE

#### 2.3.1. Small Sized Motors (1.1 kW)

The data of the first 1.1 kW motor used are given in Table 2. The machine frame is made out of aluminum. Table 3 gives the most important components of the frequency spectrum of the PWM-VSI inverter. It is a commercial type, using a special integrated circuit for producing the switching commands. Table 4 gives the audible noise emitted by the motor. The audible noise peak at 360 Hz is due to the cooling fan, rotating at 40 Hz, having nine blades, yielding  $9 \cdot 40 = 360$  Hz.

TABLE 2. Data of the first 1.1 kW induction motor

ELIN 1.1 kW	Type LKM408M02F3B
U = 220/380 V	f = 50 Hz
I = 4.5/2.6 A	n = 2800 r/min
cosφ = 0.85	IP54
Insulation Class F	17 rotor slots
24 stator slots	

TABLE 3. Largest components of the frequency spectrum of the PWM-VSI

40 (fundamental frequency)	
524	
684	
1168	
1248	
1652	
1728	
1976	
2216	
2620	

TABLE 4. Audible noise spectrum of the 1.1 kW motor supplied by the PWM-VSI

360 (fan audible noise)	
524	
724	
978	
1208	
1612	
1772	
1936	
2176	
2236	
2500	
2580	
2740	

In Table 6 the frequency components predicted by the electromagnetic analysis and the measured spectrum are compared for an other motor with rated data given in Table 5. The third column gives the nearest natural frequencies as measured by the nodal analysis technique. The first and the second column show excellent agreement. Hence, the approach accurately predicts the frequencies of the audible noise spectrum.

TABLE 5. Data of the second 1.1 kW induction motor

U = 380 V	Insulation class F
Y-connected	IP 54
I = 2.8 A	36 stator slots
P = 1.1 kW	20 rotor slots
1420 rpm	

The large components (index 1) all correspond to an excitation frequency somewhat near (within approximately 150 Hz) to a measured natural frequency, suggesting that resonance occurs. If the excitation frequency is not near a natural frequency, the corresponding audible noise level is low. Even if the electromagnetic force spectrum component is near a natural frequency, the corresponding audible noise component is not always high (index 2). This may be due to the acoustic emission of the stator assembly, a factor not accounted for in the analysis.

### 2.3.2. Medium Sized Motors (13.5 kW)

The basis for the 13.5 kW motors is a standard machine with a double cage rotor cast aluminum, as a standard design by European manufacturers. It should be stressed that different rotor bar designs as prescribed by NEMA in North-America (National Electrical Manufacturers Association) are not available in Europe [16]. The rotor bars are not insulated with respect to the rotor iron, leading to extra losses due to interbar currents. This rotor construction is required to increase the starting torque when supplying the motor from the grid as such starting problems are not present in inverter supplied machines. Therefore, current redistribution is not required and merely leads to an increase of the losses due to the harmonics of the non sinusoidal voltage.

In order to assess the influence of the current redistribution in the rotor, a special rotor is constructed with insulated round copper rotor bars.

Furthermore, the original double layer stator winding was replaced by a single layer winding. The cross-section area A of the rotor bars is chosen such that the losses at rated speed are the same as in the standard 13.5 kW motor, i.e. the dc resistance of the bars of both rotors is the same:

$$R_{dc} = \frac{\rho_{cu} l}{A_{Cu}} = \frac{\rho_{al}}{A_{Al}} \quad (4)$$

The first inverter is a standard inverter with IGBTs. The switching frequency of the components can be set from 1 to 12 kHz. The tests are done in the normal operation mode, i.e. keeping the Volts/Hz ratio constant. Due to the internal logic circuit, the inverter changes the operating switching frequency with respect to the pre-set value. Therefore, the voltage and current waveforms are monitored and recorded.

The second inverter is transistor based, having a lower switching frequency. In this inverter, the switching frequency can not be controlled. As a reference, a pure sinusoidal supply is used. Applying these combinations, the influence of the most important parameters on the audible noise may be studied.

The overall audible noise level is measured for the original standard motor with double layer stator winding. In Fig.7 the overall audible noise level at different fundamental frequencies is presented as a function of the switching frequency. As prescribed in the standards, a dB(A) filter was used.

The same measurements are repeated using the motor with the single layer winding (after rewinding the stator), and with the original rotor. As a last series of measurements, the copper bar rotor was installed.

TABLE 6. Comparison of the measured (first) and calculated (second) spectrum of the first 1.1 kW induction motor. The third column gives the nearest mechanical natural frequency

Audible noise peak	Excitation	Natural frequency
364	fan	
524	532	500-540
424 <sup>2</sup>	720	572
928	932	-
1208	1200	1198
1612 <sup>2</sup>	1626	1736
1772	1760	1736
1936 <sup>2</sup>	1920	1736
2176	2160	2280
2256 <sup>1</sup>	2266	2280
2500 <sup>1</sup>	2506	2576
2580	2586	2576
2740 <sup>1</sup>	2719	2616

- At a switching frequency of 3.6 kHz, the overall audible noise level is higher than expected in the case of fundamental frequencies up to 40 Hz. This is due to the excitation of a natural frequency of the stator by the frequency of one of the vibrations produced by the electromagnetic forces caused by the switching frequency. For the motor with double layer stator winding at higher frequencies these phenomena do not occur.
- In the case of the modified motor with the single layer stator winding, this phenomenon occurs again at 40 Hz ( $f_{\text{switch}} = 11$  kHz) and at 50 Hz ( $f_{\text{switch}} = 5.4$  kHz). This second frequency is due to the appearance of more space harmonics in this motor, that are canceled using the double-layer winding in the original motor.
- Generally the overall audible noise level decreases if the switching frequency increases. Particularly up to 6 kHz and fundamental frequencies below 50 Hz there is a large drop in the audible noise. Thus at lower motor speeds the overall audible noise is strongly reduced by applying higher switching frequencies. Once the switching frequency is above 6 kHz, the overall audible noise level is stabilized because the number of switching harmonics in the audible noise region strongly decreases.
- At higher fundamental frequencies thus at higher motor speeds the overall audible noise level decreases less if the switching frequency increases, due to the audible noise of the fan that dominates the overall audible noise level.
- If no resonance occurs between the forces caused by the space harmonics in the flux density distribution in the air gap, and the stator natural frequencies, the motor with the single layer stator winding produces less audible noise than the original motor. This is due to the more stiff type of insulation material used during rewinding: a higher class of insulation material is used, generally leading to a higher stiffness of the link between stator winding and stator iron [1, 21].
- When comparing the motor with the copper rotor, it was noted that the audible noise level was higher than with the original rotor. Some of the data can be found in Table 7. This is caused by the increased level of slotting harmonics in this machine, as the new rotor has open rotor slots, while the original one has closed ones.

When comparing the different types of supply, all three motors were loaded with 1 Nm torque. The fundamental frequency of the supplied voltage is 50 Hz. There is a difference of 1 dB(A) due to the harmonics in the 12 kHz inverter. If a switching frequency of 1 kHz is used, either IGBT or transistor based inverter, the increase is more pronounced. Clearly, an increase of the switching frequency is advantageous up to 6 kHz, but beyond 10 kHz, not much benefit should be expected.

The differences in the vertical direction of the table are far more pronounced. The inverter motor (double layer stator, abbreviation SS) can not be compared to the other two (HS: single layer stator, copper rotor; HH: single layer stator, copper rotor). However, when comparing the latter two, the influence of the slotting harmonics

becomes obvious. Furthermore, the copper rotor is not skewed, again increasing the influence of the harmonics, and thus increasing the audible noise level.

In order to show the influence of the frequency spectrum of the supplied voltage, the spectra of the voltage and the audible noise are compared. From Fig.8, the influence of the higher switching frequency on the audible noise level becomes obvious. All measurements were performed in dB without filtering the input signal of the microphone, as was done for the overall audible noise level. Apart from the level as such, pure tones may be noticed in the spectra. This is often the case in inverter supplied induction motors. As the human ear is particularly sensitive to such pure tones, the audible noise of inverter supplied machines containing such pure tones is found to be very disturbing. This problem may be cured by using random PWM techniques.

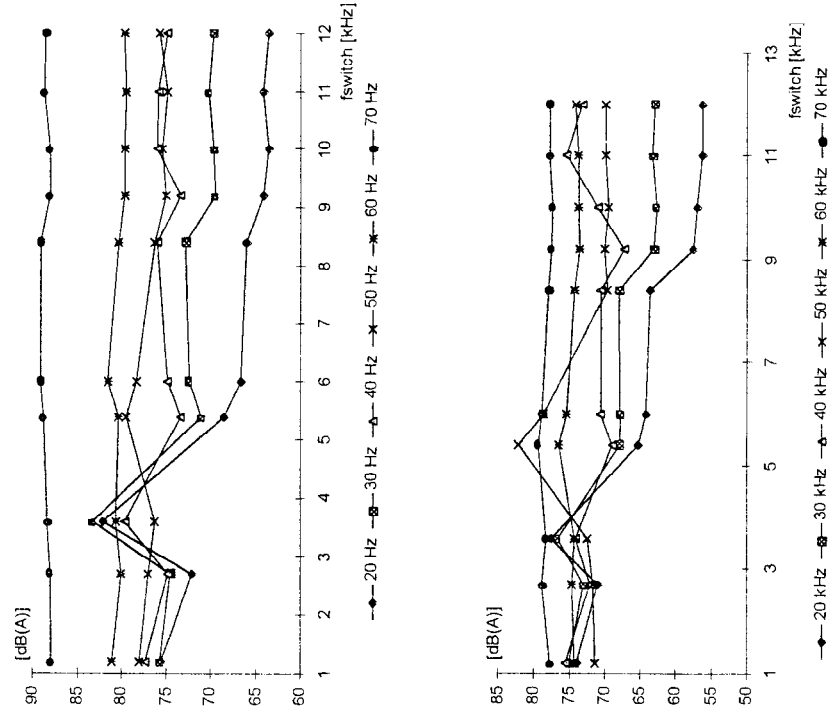


Figure 7. Overall audible noise level of the original standard motor (top) and the motor with the original stator and single layer wound stator (bottom) as a function of the IGBT-inverter switching frequency at different fundamental frequencies

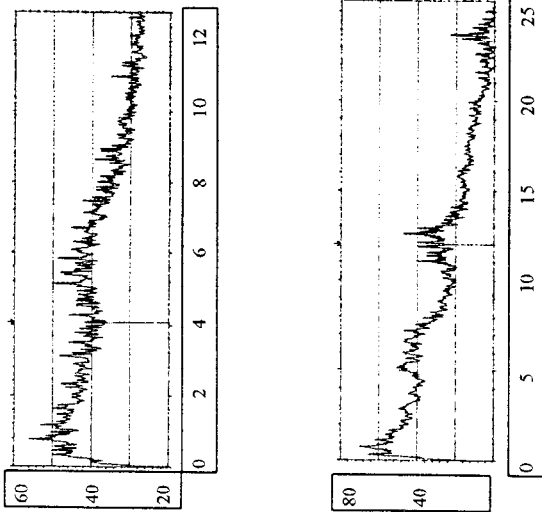


Figure 8. Frequency spectrum of the audible noise (Top: transistor inverter 1 kHz; bottom: IGBT inverter 12 kHz)

TABLE 7. Audible noise of the different motor-inverter combinations

Motor	50Hz Supply	IGBT-Inverter	IGBT-Inverter	Transistor Inverter
SS	74.8	1.2 kHz	12 kHz	1 kHz
HS	68.8	78.0	75.5	77.0
HH	76.3	71.5	69.4	74.6
		77.0	75.4	77.7

3. Large Sized Motors (90 kW)  
 the 90 kW machines three types of supply were used:

- sinusoidal supply with variable frequency (variable speed dc motor driving a synchronous generator supplying the test motor) (Fig.9);
- current source inverter (CSI);
- pulse width modulated voltage source inverter (PWM-VSI).

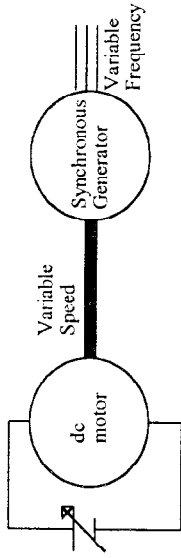


Figure 9. Set-up of the sinusoidal variable frequency supply

The first motor has a heat pipe cooling system and may be equipped with two types of rotors, one having 27, the other 28 rotor slots. The second is a standard squirrel cage induction motor.

In CSI and non-pulsed VSI having 6, 12 and 18 times the fundamental frequency are generally very pronounced. The used PWM-VSI inverter has a pulse frequency yielding harmonics having a large influence on the audible noise. The frequency of the time harmonics is in the range between 500 and 2200 Hz.

All three motors and supply types are combined. The fundamental frequency is varied from 5 Hz to 50 Hz. In order to limit the influence of the aerodynamic audible noise, the fan is removed. The motor is not loaded and the stator is Y-connected. In the above mentioned frequency range, the overall values of the audible noise (both linear and dB(A)) are measured. The frequency spectra of the supplied voltage, current and audible noise are evaluated for specific values of the supply frequency, where the audible noise level is particularly high. The combined results of all three motors and inverters are shown in Figs.10, 11 and 12.

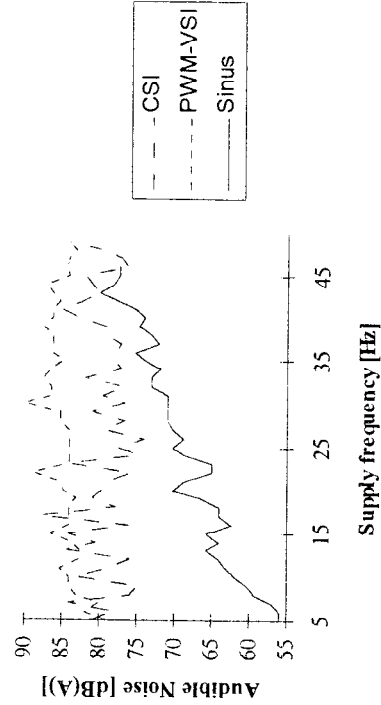


Figure 10. Audible noise of the standard induction motor for various supply types as a function of the fundamental supply frequency

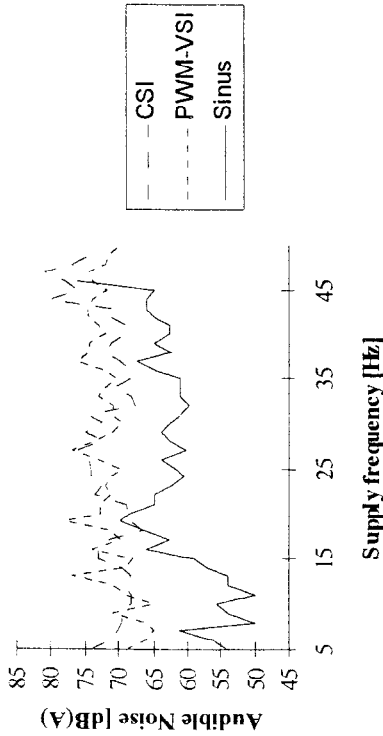


Figure 11. Audible noise of the heat pipe cooled induction motor with 27 rotor slots for various supply types as a function of the fundamental supply frequency

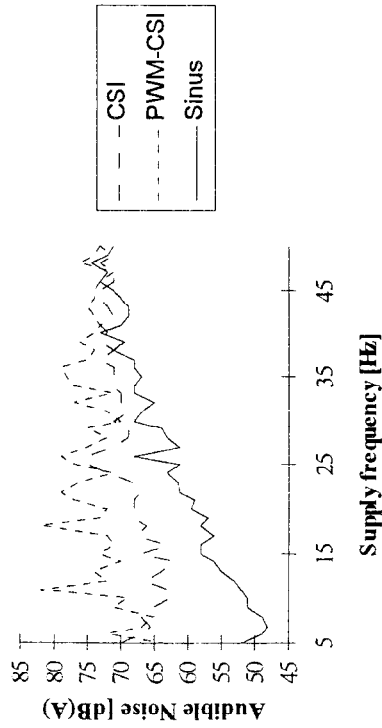


Figure 12. Audible noise of the heat pipe cooled induction motor with 28 rotor slots for various supply types as a function of the fundamental supply frequency

As a general conclusion, it can be seen that the influence of the supply harmonics the audible noise becomes more pronounced in the lower frequency range. The rease may be as high as 30 dB, the PWM-VSI being the least favorable in this re-ct.

In Fig.13 it is shown that with a sinusoidal supply, the 28 slot motor has approximately the same emitted audible noise as the standard motor. The 27 slot motor y have either positive or negative deviations that may be as high as 10 dB(A). erefore, a general conclusion with regard to the advantage of odd or even slot rbers is not possible, when the supply frequency is controlled.

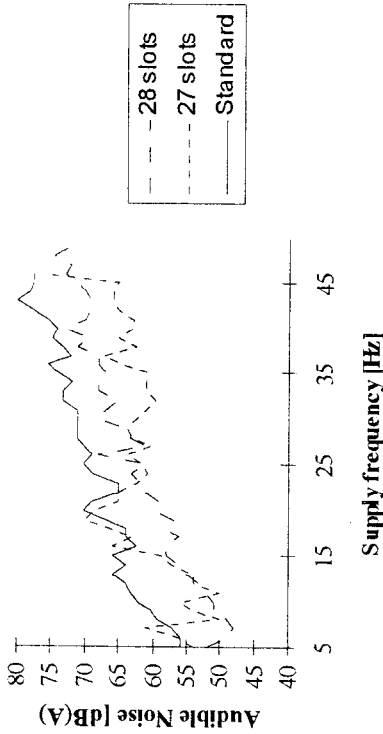


Figure 13. Audible noise of the three induction motors for sinusoidal supply as a function of the fundamental supply frequency

With the 27 slot motor, resonances are found in the frequency range of 16 to 20 Hz due to saturation harmonics and due to the stator fundamental and the second rotor slotting harmonic. The resonance is due to the specific number of slots. An increase of 13 dB(A) of the audible noise is found. This resonance causes with all supply types the highest audible noise level and is the real disadvantage of the odd number of rotor slots, when a speed controlled system is used. The increase of the audible noise level at 37 Hz is caused by the resonance excited by the combination of the stator fundamental field and the third rotor slotting harmonic. The resonance problems seen with the sinusoidal supply are with inverter supply mystified by the audible noise increase caused by the supply harmonics.

The resonance frequencies as measured using the modal analysis technique for the heat pipe cooled motor stator are given in Table 8. With the CSI, the audible noise is to a large extent independent of the motor type.

TABLE 8. Natural frequencies of the heat pipe cooled motor using the modal analysis technique

Natural frequencies	
1800	
2000	
2500	
2800	
3000	
3600	
4000	
4500	
5000	

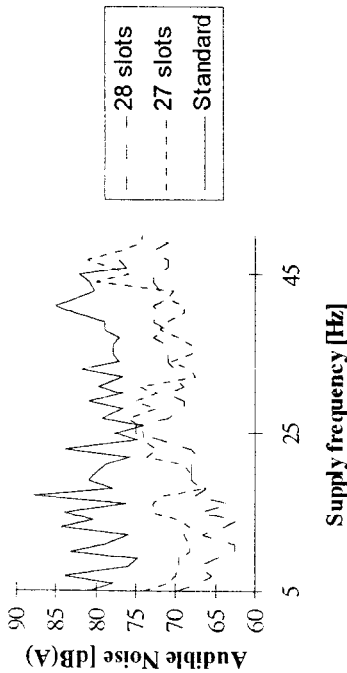


Figure 14. Audible noise of the three induction motors for CSI supply as a function of the fundamental supply frequency

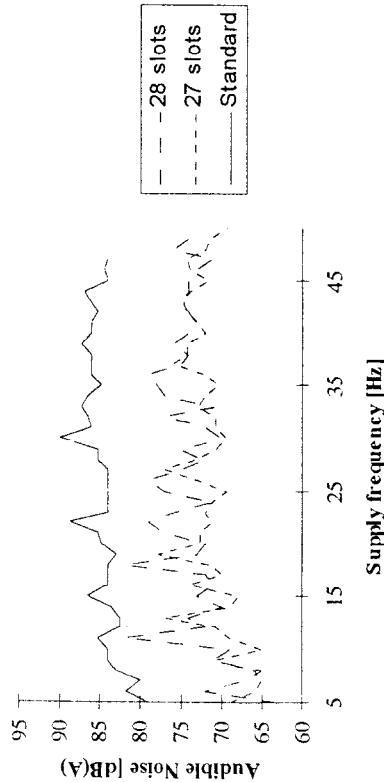


Figure 15. Audible noise of the three induction motors for PWM-VSI supply as a function of the fundamental supply frequency

When analyzing the audible noise differences in the VSI-PWM supplied 28 slots motor, the inverse tendency is noted as this motor shows a large audible noise increase (gs. 14 and 15). This is due to the supplementary harmonics caused by the earthing of neutral conductor.

In Fig.16 the audible noise spectrum of the 27 slot heat pipe cooled motor is shown at a sinusoidal supply frequency of 45 Hz. The audible noise due to the combination of the stator fundamental and the rotor slotting harmonics contains following frequencies:

- f = 505-685 Hz (1-st rotor slotting harmonic)
- f = 1280 Hz (2-nd rotor slotting harmonic)
- f = 2500 Hz. (3-rd/4-4h rotor slotting harmonic-resonance)
- f = 3100 Hz. (4-4h/5-4h rotor slotting harmonic)

The high audible noise peak at 2500 Hz is due to the resonance as one of the mechanical natural frequencies is particularly close. Also 3100 Hz is one of the natural frequencies.

The frequency spectrum of the audible noise generated by the motor supplied by the CSI shows a low spectrum at high frequencies with high peaks in the low frequency range (Fig.17). The 200 and 400 Hz audible noise components are caused by the 5th and 7th, respectively 11th and 13th current time harmonics, inducing currents in the rotor at 6, respectively 12 times the fundamental frequency.

Fig.18 shows the audible noise when using the sinusoidal supply at 36 Hz. The typical sound frequencies are again due to the rotor slotting harmonics.

- f = 636-708 Hz (1st rotor harmonic)
- f = 1345-1489 Hz (2<sup>nd</sup> rotor harmonic)
- f = 2054-2198 Hz (3<sup>rd</sup> rotor harmonic)

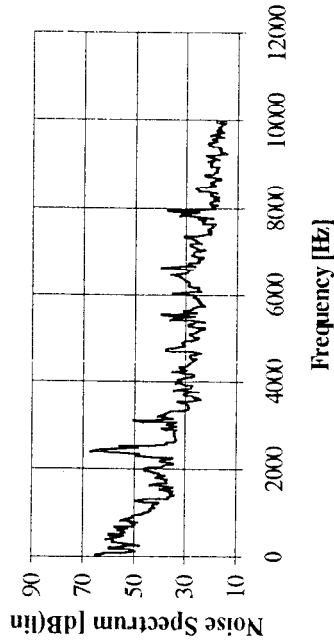


Figure 16. Audible noise frequency spectrum of the heat pipe cooled induction motor with 47 slots supplied by the sinusoidal supply at 45 Hz

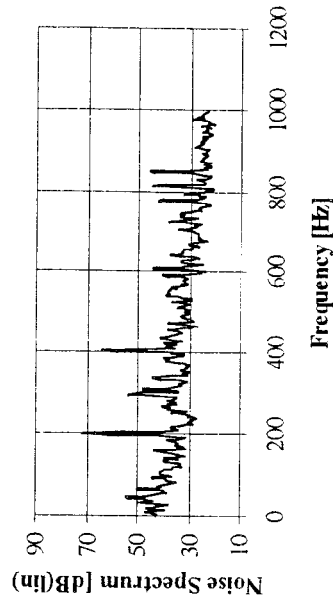


Figure 17. Audible noise frequency spectrum of the heat pipe cooled induction motor with 47 slots supplied by the CSI at 34 Hz

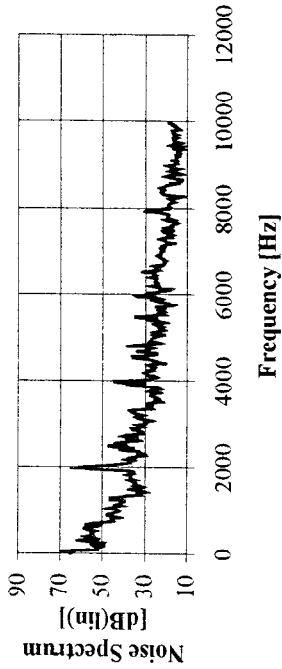


Figure 18. Audible noise frequency spectrum of the heat pipe cooled induction motor with 47 slots supplied by the sinusoidal supply at 36 Hz

This spectrum may be compared to the one of the PWM-VSI supplied motor (Fig. 19). As resonance occurs at 2000 Hz, a minor excitation, as e.g. due to the 4<sup>th</sup> and 7<sup>th</sup> time harmonic with an amplitude of approximately 4 % of the fundamental time harmonic of the current with the PWM-VSI supply may lead to high audible noise levels. Here the increase is 30 dB. As the frequency spectrum of the current of a PWM inverter only alters slightly as the supply frequency changes, these resonances dominate the audible noise frequency spectra at all speeds.

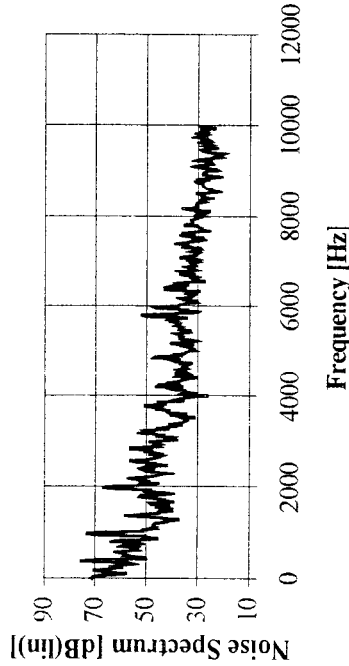


Figure 19. Audible noise frequency spectrum of the heat pipe cooled induction motor with 47 slots supplied by the PWM-VSI at 34 Hz

However, a resonance situation is not obligatory. Figs. 20 and 21 show for fundamental frequencies of 16 Hz sinusoidal and 15 Hz PWM-VSI, the audible noise spectrum emitted by the 27 rotor slots heat pipe cooled motor. The spectrum is dominated by a component at 272 Hz coming from the combination of the second rotor time harmonic and a component due to saturation. The supplementary time harmonics, generate further frequencies, being multiples of the pulse frequency (1260 Hz, 1890 Hz, 2520 Hz).

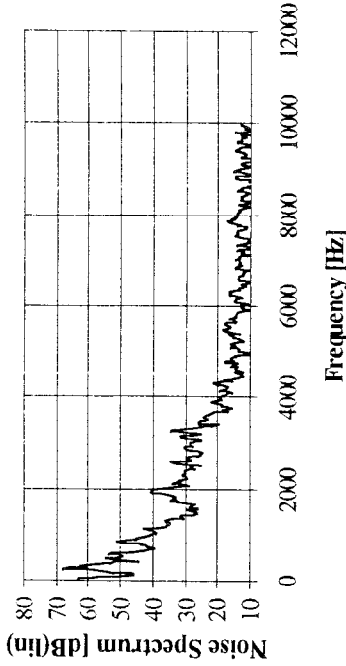


Figure 20. Audible noise frequency spectrum of the heat pipe cooled induction motor with 47 slots supplied by the sinusoidal supply at 16 Hz

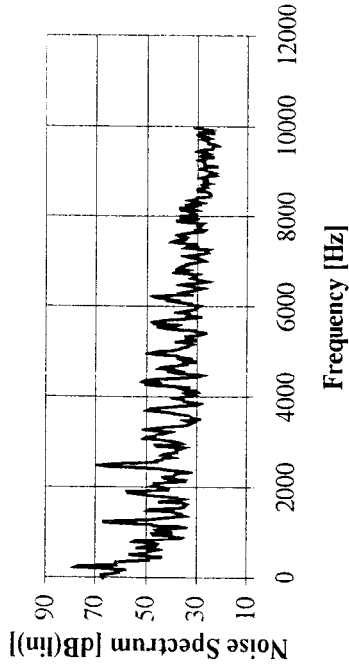


Figure 21. Audible noise frequency spectrum of the heat pipe cooled induction motor with 47 slots supplied by the PWM-VSI at 15 Hz

### 3. Mechanical Aspects - Calculation of Eigenfrequencies and Modes

#### 3.1. SEMI-ANALYTICAL STUDY

A lot of semi-analytical methods are developed over the years for predicting the stator natural frequencies of electrical machines. H. Jordan [5] started the analysis and a lot of elaboration of his basic work may be found [7-9]. The most advanced semi-analytical study is the work by S.P. Verma [22, 23]. He replaced the simple ring model by a three dimensional system as in general, stators of electrical machines are subjected to axial, torsional and radial vibrations. All these vibrations can be excited simultaneously during the machine operation. In the analysis, both stator core and frame were treated rigorously, while teeth and windings were considered as additional masses. It is well known that teeth and windings have a large effect on the values of resonant frequencies

6

stators. Therefore, an accurate simulation of teeth and windings is essential. In addition, the analysis is limited to only special modes along the machine length.

In actual practice, the longitudinal modes are a combination of these special modes. A better way is found using the energy method, in which the simulation of the boundary conditions is avoided, while considering teeth and windings rigorously. The energy method also permits accurate simulation of the actual modes of vibrations along the machine length. A brief description of an analytical method based on the three-dimensional theory of elasticity and using the energy method is presented here.

According to the three dimensional theory of elasticity, the kinetic energy  $E_{kin}$  and potential energy  $E_{pot}$  of a cylindrical shell of length  $L$ , inner radius  $r_i$  and outer radius  $r_o$ , can be obtained in the form:

$$E_{kin} = \frac{\rho}{2} \int_{z=0}^z \int_{r=0}^r \int_{\theta=0}^{\theta=2\pi} \left[ \left( \frac{\partial u}{\partial t} \right)^2 + \left( \frac{\partial v}{\partial t} \right)^2 + \left( \frac{\partial w}{\partial t} \right)^2 \right] r dr d\theta dz \quad (20)$$

d

$$E_{pot} = \frac{\rho}{2} \int_{z=0}^z \int_{r=0}^r \int_{\theta=0}^{\theta=2\pi} \left[ \sigma_r \epsilon_r + \sigma_\theta \epsilon_\theta + \sigma_z \epsilon_z + \tau_{rz} \gamma_{rz} + \tau_{r\theta} \gamma_{r\theta} + \tau_{\theta z} \gamma_{\theta z} \right] r dr d\theta dz \quad (21)$$

ns.20 and 21 can be used to determine the energy components of both stator-yoke and frame-shell by direct substitution of the proper parameters.

Energy components in teeth, windings and cooling ribs can be obtained by treating these parts as discrete beam-type elements attached to the body of the stator. Considering the realistic relative dimensions of these elements in electrical machines, it is sufficient to use the following approximate expressions of kinetic and potential energies of a cantilever.

$$E_{kin} = \frac{\rho}{2} \Lambda \int_{z=0}^z \int_{r=0}^r \left[ \left( \frac{\partial u_b}{\partial t} + r_c \frac{\partial^2 w_b}{\partial z \partial t} \right)^2 + \left( \frac{\partial v_b}{\partial t} + \frac{\partial^2 w_b}{r_b \partial \theta \partial t} \right)^2 + \left( \frac{\partial w_b}{\partial t} \right)^2 + R_c^2 \left( \frac{\partial^2 w_b}{\partial z \partial t} \right)^2 + R_{cp}^2 \left( \frac{\partial^2 w_b}{\partial \theta \partial t} \right)^2 \right] dz \quad (22)$$

1

$$E_{pot} = \frac{1}{2} EA \int_{z=0}^z \int_{r=0}^r \left[ \left( \frac{\partial u_b}{\partial z} \right)^2 + 2r_c \frac{\partial v_b}{\partial z} \frac{\partial^2 w_b}{\partial z} + R_c^2 \frac{\partial^2 w_b}{\partial z^2} + R_{\theta\theta}^2 \left( \frac{\partial^2 w_b}{\partial z^2} \right)^2 \right] dz + \frac{1}{2} GJ \int_{z=0}^z \int_{r=0}^r \left[ \left( \frac{\partial^2 w_b}{r_b \partial z \partial \theta} \right)^2 \right] dz \quad (23)$$

677

Using the ordinary Ritz method, the components of displacement are approximated by the following finite double power series:

$$u = \sum_{i=1}^M \sum_{j=1}^M \sum_{k=0}^{\infty} (a_{ijk} \cos k\theta + b_{ijk} \sin k\theta) z^i r^j \quad (24)$$

$$v = \sum_{i=1}^M \sum_{j=1}^M \sum_{k=0}^{\infty} (c_{ijk} \cos k\theta + d_{ijk} \sin k\theta) z^i r^j \quad (25)$$

$$w = \sum_{i=1}^M \sum_{j=1}^M \sum_{k=0}^{\infty} (e_{ijk} \cos k\theta + f_{ijk} \sin k\theta) z^i r^j \quad (26)$$

where  $a_{ijk}$ ,  $b_{ijk}$ ,  $c_{ijk}$ ,  $d_{ijk}$ ,  $e_{ijk}$  and  $f_{ijk}$  are coefficients of the expression that also serve as the generalized co-ordinates of the system.  $M$  and  $N$  are two integers and determine the size of the mathematical model representing the vibrating system. These two integers determine the accuracy of calculation. In deciding on the shape of the displacement distribution, several considerations related to the stator construction and the nature of vibrations of stators are taken into account. Having assumed the mode shape functions for the displacements  $u$ ,  $v$  and  $w$ , the total kinetic and potential energies of the stator can be readily obtained in terms of the generalized co-ordinates of the system, before they are introduced into the Lagrange's equation for conservative systems. This leads to a set of homogeneous equations. The coefficient matrix of these equations yields the frequency equation of the stator. The frequency equation can be made dimensionless.

Although this analytical formulation is very tentative, the calculation time involved in solving the equation system is large and may take several hours of computing time. Furthermore, it is essentially an analysis method, depending on knowledge from experiments on existing systems, that are, in a certain way, extrapolated. It would not, for instance, be possible to extrapolate the results obtained from cylindrical machine, to machines with a square shaped lamination, as found in many servomotor designs.

### 3.2. FINITE ELEMENT ANALYSIS

Apart from the principal disadvantages mentioned above, a specific disadvantage of analytical methods when analyzing the natural frequencies, is its lack of detail. All classical methods assume the machine stator to be uniformly cylindrical. The effects of air-ducts spacers, the connecting box, the non-uniform stator core thickness and other irregularities are neglected. The machine mounting significantly influences the natural frequencies and that also introduces asymmetries.

In order to account for all detailed structure dimensions, the finite difference method [24] as well as the finite element method [25, 26] may be used. Both numerical methods suffered from the time consuming data introduction (geometry input and grid generation). Therefore the coupling of these mathematical methods with modern

computer Aided Design techniques is a must in order to obtain the flexibility required easily vary the machine parameters during the design stage.

### 2.1. Finite Element Method

the finite element theory states that the behavior of the finite element model converges the behavior of the real structure if a sufficiently large number of finite elements are used. The accuracy of a particular finite element model, compared to the "true" behavior of the actual structure, depends on a number of considerations, including:

- number and location of the nodes;
- type of elements used in the model;
- size and shape of the individual elements;
- numerical procedure used to solve the mathematical equations;
- techniques employed in recovery of derived results.

The first three considerations are controlled by the user and may be described as modeling techniques". The last two are, when employing prewritten finite element software packages, not generally user-controlled. Therefore, they are characteristics of a finite element analysis computer program.

Various approaches can be used to implement the finite element method. For natural analysis, these approaches are generally classified as:

- displacement (stiffness);
- force (flexibility);
- mixed methods.

The classification depends upon the parameters selected as the unknowns in each formulation. In the stiffness method, nodal displacements are selected as unknowns. Redundant forces are unknown in the flexibility formulation, and a mixture of displacements and forces are unknown in the mixed method. Most general purpose finite element programs employ the stiffness method. The equations solved to determine unknown displacements are expressed in matrix form.

A dynamic analysis of a mechanical structure, is based on the equilibrium of forces in the nodes of the mesh:

$$[F] = [K][X] \quad (27)$$

where the applied nodal forces  $[F]$  are related to the unknown nodal displacements  $[X]$  through the structural stiffness matrix  $[K]$ . When analyzing the natural frequencies and modal shapes of a structure, only inertia forces are acting on the structure:

$$[F] = [M][\ddot{X}] = -\omega^2[M][X] \quad (28)$$

where  $\omega$  is one of the natural pulsations and  $[M]$  the mass matrix. The mass matrix  $[M]$  and the stiffness matrix  $[K]$  are functions of the geometry of the structure and of the material parameters (e.g. specific mass  $\rho$ , elasticity modulus  $E$ , Poisson coefficient  $\nu$ ).

Substituting Eq.28 into Eq.27 yields the eigenvalue problem to be solved in order to find the natural frequencies and the modal shapes of the structure. In practice, three steps may be distinguished in the finite element method.

In the preprocessing step, the model definition is elaborated. The following data have to be provided to the finite element program:

- geometry of the structure;
- coordinates of the nodes;
- geometry of the elements;
- connectivity of the elements;
- material properties assigned to elements;
- coupling of nodes to the same displacement;
- set of constrained nodes with applied displacements.

This list is not restricted, as sometimes more elaborated data sets are required (e.g. temperature dependent parameters).

During this preprocessing stage, the first, and probably the most significant advantage of combining the finite element calculation method with graphical Computer Aided Design techniques is found. The input of the large amount of geometrical data, needed for accurately representing stator slots, yoke, frame, cooling ribs, connecting box, etc., was enormously time consuming when done in a classical, numerical way.

After giving the geometrical data and the material properties, the boundary conditions are supplied to the program. Apart from the introduction of coupling nodes to the same displacements, the set of constrained nodes with applied displacements, due to the machine mounting, has to be developed.

Furthermore, the adaptation of the existing models is readily performed by changing the drawings and different boundary conditions for the same motor may be used without much effort.

During the solution process, the complete stator is divided into a set of elements having relatively simple geometrical shapes. Most modern finite element programs offer the possibility of using a variety of element shapes. After the lay-out of the finite element division, often done semi-automatically, or automatically, the assembly of the matrices representing the structure and their optimization in order to minimize the calculation time and storage requirements is performed by the program.

Then the finite element solver is started and the results for the displacements (eigenmodes) and the natural frequencies (eigenvalues) are found, using specialized mathematical techniques taking into account sparsity, renumbering techniques and other algorithms for gaining time and computer memory.

Two steps may be distinguished when speaking about finite element post-processing in mechanical problems:

- determination of derived quantities (transient displacements, accelerations, internal forces, stresses and strains);
- graphical representation of the modal shapes.

As the interest is in the analysis of the natural frequencies and the modal shapes of structure, the possibility of the graphical representation of the modal shapes is extremely important, as it supplies the fast interpretation of the results, that is impossible for users of classical finite element calculations. Furthermore, as both geometry of the structure and eigenmodes are known, the first may be used as a reference for plotting the various modal shapes.

The finite element technique is compared with classical calculation methods, that regard the stator to be uniformly cylindrical. The following advantages may be stressed:

- accurate representation of the stator iron cross-section, including stator teeth;
- asymmetrical stator structure due to the air duct spacers, the non-uniform stator core thickness, the connecting box, the mounting and other irregularities are accounted for;
- actual boundary conditions due to the machine mounting can be taken into consideration, that is impossible in classical analysis techniques regarding the stator as being suspended freely: it is evident that both eigenvalues and eigenmodes are influenced by the mounting.

### 2.2. Practical examples

The finite element approach is used to calculate the natural frequencies of a 1.1 kW three phase squirrel cage induction motor. The rated data are given in Table 2. The stator frame material is aluminum. Fig. 22 represents the grid used. In Table 9 the natural frequencies between 1,000 and 6,500 Hz are shown.

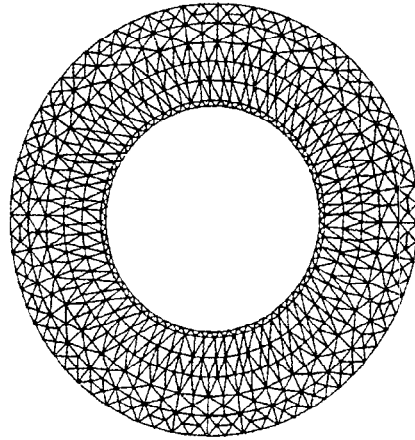


Figure 22. Finite element grid of the 1.1 kW motor

The stator teeth are accounted for. As the elasticity modulus of copper is small in respect to the modulus of steel, the mass supplement due to the windings is more important than the supplementary stiffness introduced by it. However here both

quantities are accounted for. The end windings are represented by masses added at the end of each slot. These adaptations to the model were necessary for the small motor as the influence of the windings on the natural frequencies is more important for lower machine ratings. In Figs.23, 24, 25 and 26 some of the corresponding eigenmodes are shown. Clearly the simple displacement geometries, as proposed in literature are not found in practice. This is particularly due to the influence of the machine mounting that becomes more important as the number of the eigenmode is higher.

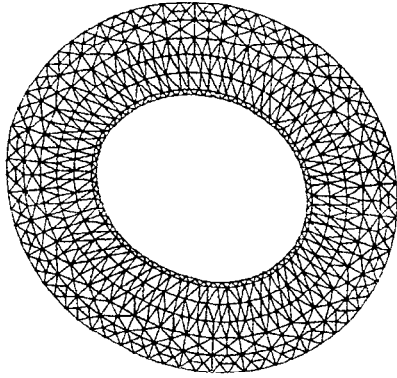


Figure 23. Eigenmode 2 of the 1.1 kW motor

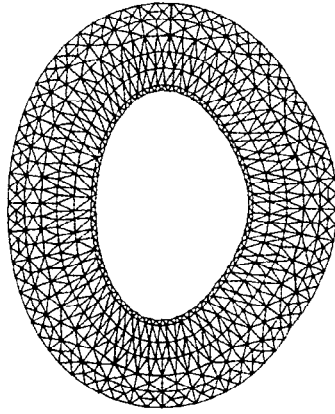


Figure 24. Eigenmode 3 of the 1.1 kW motor

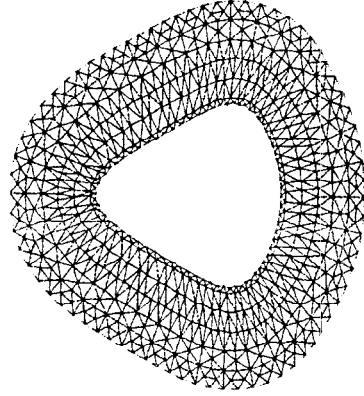


Figure 25. Eigenmode 4 of the 1.1 kW motor

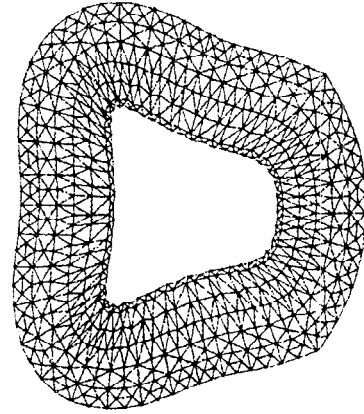


Figure 26. Eigenmode 6 of the 1.1 kW motor

TABLE 9. Calculated natural frequencies of the 1.1 kW motor

Mode number	Frequency
1	1122
2	1474
3	2515
4	2695
5	3468
6	4159
7	4930
8	5120
9	5552
10	6357

## EXPERIMENTAL VERIFICATION

The experimental verification of the natural frequencies of a mechanical structure is generally performed using the modal analysis method [27-30]. In Table 10 the experimental results of a 22 kW machine are given, that can be compared to the finite element results. The correspondence is quite good except for two natural frequencies that are not visible in the experimental data. This may be due to the fact that the accelerometer is mounted in one of the nodes of the considered mode.

TABLE 10. Calculated natural frequencies of the 22 kW motor

Mode number	Measured natural frequencies	Calculated natural frequencies
1	1106	1041
2	-	1477
3	2552	2562
4	2900	2590
5	4632	-
6	5080	4831
7	5664	5323
8	5864	5879
9	6848	6828
10	6976	7021

## Conclusions

The audible noise peak corresponding to one of the components of the stator magnetically generated forces is not large, except if its frequency is near a natural frequency of the stator. Even if the frequency of a force component and a natural frequency of the stator assembly matches, the corresponding audible noise level is not always high. It may be limited by damping effects or by acoustic emission characteristics of the stator.

The audible noise is influenced both by the inverter switching frequency and the stator construction. At high speeds, the audible noise of the fan dominates and the influence of the switching frequency is rather limited. At lower speed, a switching

frequency of 10 kHz or more leads to values of the audible noise level that are comparable to those found when using a sinusoidal supply. The influence of the flux density space harmonics is much more important. A good winding lay out, skewed rotor bars and closed rotor slots are beneficial for the audible noise level. Improved PWM switching strategies may help to avoid pure tones, that are particularly found to be disturbing by the human ear, as it is very sensitive to such pure tones.

In general, a high switching frequency improves the audible noise and losses, although precautions have to be taken to avoid resonances when looking at the audible noise. The construction of the motor is key, and all measures should be taken to avoid space harmonics. Avoiding space harmonics is more important than the reduction of time harmonics obtained by an increased switching frequency. Both theoretical (finite elements) and experimental techniques may be employed to analyze the resonant data of the stator structure.

## 5. Acknowledgements

The authors are grateful to the Belgian "Nationaal Fonds voor Wetenschappelijk Onderzoek" for its financial support for this work and Institute for Science and Technology of Flanders (IWT-Vieth).

## 6. References

- Verdyck, D. and Belmans, R. (1994) An acoustic model for a permanent magnet machine: modal shapes and magnetic forces, *IEEE Transactions on Industry Applications* **30**, 6, 1625-1631.
- Belmans, R., Verdyck, D., Geysen, W. and Findlay, R. (1991) Electromechanical analysis of the audible noise of an inverter-fed squirrel-cage induction motor, *IEEE Transactions on Industry Applications* **27**, 3, 539-544.
- Belmans, R., Geysen, W. and Verdyck, D. (1992) The use of the stator's modal shapes in the calculation of its vibrations, *International Workshop on Electric and Magnetic Fields*, Liège, 66.1-66.6.
- Verdyck, D., Belmans, R. and Geysen, W. A model for the induced mechanical vibrations in the stator of an inverter fed electrical machine, *17th International Seminar on Modal Analysis*, K.U.Leuven, 871-885.
- Jordan, H. (1950) *Geraätschirme Elektromotoren*, W. Girardet Verlag, Essen, Germany.
- Belmans, R., Geysen, W., Tuinman, E. and Gordens, J.C.A.M. (1992) Vibration aspects of the design of a new generation of dc motors for the propulsion of submarines, *IEEE Industry Applications Society Annual Meeting*, Houston, Texas, 79-85.
- Staiger, A. and Jordan, H. (1962) Der Einfluß des Gehäuses auf das Schwingungstechnische Verhalten des Ständers von Drehstrommaschinen, *AEÜ Mitterlungen*, 194-205.
- Verma, S.P. and Girgis, R.S. (1973) Resonance frequencies of electrical machines stators having encased construction, Part I and II, *IEEE PAS-92*, 1577-1593.
- Elison, A.J. and Moore, C.J. (1968) Acoustic noise and vibrations of rotating electrical machines, *Proc.IEE* **115**, 1633-1640.
- Tsvitse, P.J. and Weishmann (1971) Polyphase induction motor noise, *IEEE Transactions on Industrial General Applications* **GA-7**, 339-359.
- Landy, C.F. (1975) An investigation into some aspects of noise and vibration produced in rotating electric machines, *Transactions SA Institute of Electrical Engineers*, 190-197.
- Gießler, F. and Sattler, Ph.-K. (1988) Magnetic noise of induction machines by inverter supply, *Proceedings of the International Conference on Electrical Machines, ICEN-88*, Pisa (Italy), 611-616.

13. Gießler, F. (1988) *Asynchronmaschinen mit konventionellen und Wärmerohrkühlung am U- und L-Umrichter, Vergleich hinsichtlich der Ausnutzung, der Verluste und der Geräusche*. Ph.D. Thesis, RWTH-Aachen, Germany.
14. Zubek, J., Abbondanti, A. and Norby, C.J. (1975) Pulsewidth modulated inverter motor drives with improved modulation, *IEEE Transactions on Industrial Applications IA-11*, **6**, 695-703.
15. Bosse, B.K. (1991) *Modern Power Electronics: Evolution, Technology and Applications*, IEEE Press, New York, USA.
16. Sen, P.C. (1989) *Principles of Electrical Machines and Power Electronics*, Wiley & Sons, New York-Chichester-Brisbane-Toronto-Singapore.
17. Boller, H.W. and Jordan, H. (1963) Über die phasenrichtige Addition der nutharmomischer Wicklungsoberrfelder und der Nutzungsoberfelder bei phasenreichen Mehrphasenwicklungen, *ETZ*, **4**, 84, 235-238.
18. Belmans, R., Geysen, W., Bailly, G. and Sattler, Ph.K. (1990) Theoretical and experimental analysis of the audible noise in an inverter fed squirrel cage induction Motor, *Proc. ICEM-90*, **Part II**, Cambridge, Massachusetts, 485-490.
19. Muster, J., Budig, P.K., Belmans, R. and Geysen, W. (1995) Audible noise in speed-controlled inverter-fed medium-sized induction motors, *ETEP*, Eurel publication **5**, **1**, 5-13.
20. Früchtenicht, J., Jordan, H. and Seinsch, H. (1982) Exzentritätsfelder als Ursache von Laufstabilitäten bei Asynchronmaschinen: Teil I und II", *Arch. Elektrotechnik* **65**, 271-292.
21. Verdyck, D. and Belmans, R. (1994) A vibrational model using modal shapes and magnetic forces: experimental results for a permanent magnet machine, *Archiv für Elektrotechnik* **77**, 383-389.
22. Grgis, R.S. and Verma, S.P. (1981) Methods for accurate determination of resonant frequencies and vibration behavior of stators electrical machines, *Proceedings IEE* **128**, **part B**, 1-11.
23. Verma, S.P. Vibration behaviour of stators of electrical machines, *Proceedings of the NATO Advanced Research Workshop*, NATOASI Series E **148**, 499-513.
24. Thomson, W.T. (1977) *Vibration and Noise in Small-power Electric Motors*, M.Sc. Thesis, Strathclyde University.
25. Shumilow, J.A. (1974) Calculating stator vibrations in electrical machines, *Proc. of the International Conference on Electrical Machines*, London, B3.1-B3.5.
26. Yang, S.J. (1978) Finite element method in evaluating the stator natural frequencies of small machines, *Proc. of the International Conference on Electrical Machines*, Brussels, G3/8.1-G3/G3.8.
27. Formenti, D. (1977) Analytical and experimental model testing, *Seminar on modal analysis K.U.Leuven*.
28. Brown, D., Garbon, G. and Ramesey, K. (1977) Survey of excitation techniques applicable to the testing of automotive structures, *SAE paper 770029*.
29. Halvorsen, W. and Brown, D. (1977) Impulse technique for structural frequency response testing, *Sound & Vibration*.
30. Brown, D., Allemang, R., Zimmerman, R. and Mergery, M. (1979) Parameter estimation techniques for modal analysis, *SAE paper 790221*.

#### Dr. J.M. BELMANS

Dr. J.M. Belmans received his M.Sc. degree in electrical engineering in 1979, his Ph.D. degree in 1984 and his doctorate in 1989, all three from the K.U. Leuven, Belgium. He was awarded the Habilitation in 1993, the RWTH in Aachen, Germany. Currently, he is a full professor in the K.U. Leuven, teaching electrical machines, CAD in magnetics and variable speed drives. His research interests include electrical machine design (permanent magnet and induction machines), computer aided design and optimization, vibrations and audible noise in variable speed drives and advanced control in electrical drives. He was the Director of the NATO Advanced Research Workshop on Vibrations and Audible Noise in Alternating Current Machines (August 1986). He worked in the laboratory for Electrical Machines of the RWTH-Aachen, Germany, as a Von Humboldt Fellow (October-September 1989). From October 1989 until September 1990, he was visiting professor at McMaster University, Hamilton, Ontario, Canada. He held the chair of the Anglo-Belgian Society at London University for academic year 1995-1996. He is the international secretary of the International Conference on Electrical Machines. He is author of more than 100 papers in scientific journal and reviewed international conferences. Dr. R. Belmans is a senior member of the IEEE (USA), the IEE (United Kingdom) and the Koninklijke Vlaamse Ingenieursvereniging (KVIV-Belgium).